THE JOURNAL OF PHYSICAL CHEMISTRY A

Article

pubs.acs.org/JPCA

Detection of Mercury–TpT Dinucleotide Binding by Raman Spectra: A Computational Study

Ladislav Benda, Michal Straka, Vladimír Sychrovský, and Petr Bouř*

Institute of Organic Chemistry and Biochemistry, Academy of Sciences, Flemingovo nám. 2, 16610 Praha 6, Czech Republic

Yoshiyuki Tanaka

Laboratory of Molecular Transformation, Graduate School of Pharmaceutical Sciences, Tohoku University, 6-3 Aza-Aoba, Aramaki, Aoba-ku, Sendai, Miyagi 980-8578, Japan

ABSTRACT: The Hg^{2+} ion stabilizes the thymine–thymine mismatched base pair and provides new ways of creating various DNA structures. Recently, such T–Hg–T binding was detected by the Raman spectroscopy. In this work, detailed differences in vibrational frequencies and Raman intensity patterns in the free TpT dinucleotide and its metal-mediated complex $(TpT{\cdot}Hg)_2$ are interpreted on the basis of quantum chemical modeling. The computations verified specific marker Raman bands indicating the effect of mercury binding to DNA. Although the B3LYP functional well-describes the Raman frequencies, a dispersion correction had to be added for all atoms including mercury to obtain realistic geometry of the $(TpT{\cdot}Hg)_2$ dimer. Only then, the DFT complex structure agreed with those obtained with the wave function-based MP2 method. The aqueous solvent modeled as a polarizable continuum had a minor effect on the dispersion interaction, but it stabilized conformations of the sugar and phosphate parts. A generalized definition of internal coordinate force field was introduced to monitor covalent bond mechanical strengthening and weakening upon the Hg^{2+} binding. Induced vibrational frequency shifts were rationalized in terms of changes in electronic structure. The simulations thus also provided reliable insight into the complex structure and stability.

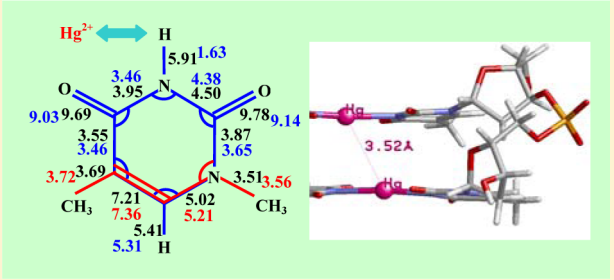

INTRODUCTION

Interactions of nucleic acids (NA) with transition metal ions attract attention in research of both natural and artificially designed oligonucleotides. Chemical, mechanical, and electronic properties of metal–NA complexes promise new applications in nanotechnology.[1−12] NA base pairs can be stabilized by specific metal–NA[13] and metal–metal[14] interactions. Some structures, such as the T–Hg–T base pair studied in this work, can be incorporated into double-strand DNA or RNA without significantly perturbing the duplex structure. Yet, the DNA geometry seems to be perturbed particularly locally at the binding site, which provides specific changes in the Raman spectra.[13] The Raman spectroscopy thus not only represents a convenient alternative to nuclear magnetic resonance (NMR)[15,16] but also complements the information on the T–Hg–T complex formation.

Mercury is also known as a toxic metal affecting biochemical properties of DNA.[17−22] Hg^{2+} preferentially binds to the nitrogen atoms of the bases.[23] Specific Hg^{2+} binding to the imino nitrogen (N3) of thymine (T) upon releasing the imino proton (H3) was proposed already in 1960s,[18,24] including the possibility of forming the T(N3)–Hg–T(N3) link.[25] Crystal structure of a 2:1 complex of 1-methylthymine with Hg^{2+} confirmed the existence of the T(N3)–Hg–T(N3) link and showed that the T–Hg–T residue may adopt nearly planar geometry.[25] Formation of T–Hg–T links in DNA molecules upon the addition of Hg^{2+} was also indicated with circular dichroism (CD) and ^{1}H nuclear magnetic resonance (NMR).[26,27] However, this mode of Hg^{2+} binding to DNA was unequivocally confirmed only lately.[4,15,28]

The stabilization of NA by Hg^{2+} opens a way to surprising applications, such as the colorimetric detection of mercury[29] or cysteine[30] or synthesis of molecular wires based on NAs containing one-dimensional arrays of mercury atoms.[31] It was suggested that the interaction of neighboring T–Hg–T base pairs could increase the hole transfer efficiency in a DNA.[32] However, such an enhancement of DNA conductivity by the T–Hg–T base pairs has not been observed so far.[33]

Previous quantum chemical computations revealed the electronic structure and confirmed the stability of the T–Hg–T link. UV absorption spectra suggest that the Hg···Hg interaction in stacked base pairs substantially stabilizes the lowest unoccupied molecular orbital,[34] which readily explains the Hg-induced changes in experimental UV spectra of a DNA

Received: May 9, 2012
Revised: June 12, 2012
Published: July 17, 2012

dx.doi.org/10.1021/jp3045077 | J. Phys. Chem. A 2012, 116, 8313–8320

duplex containing the T−T mismatches.[4] The apparently counterintuitive occurrence of two positively charged Hg atoms being in relatively close contact (~3.5 Å) in consecutive T−Hg−T base-pair steps was explained in a recent study conducted in our laboratory by the dominance of the dispersion (van der Waals) interaction over the electrostatic repulsion.[14] By analyzing the interaction energy of two consecutive U−Hg−U base pairs (an RNA equivalent of T−Hg−T), we found that a weak binding of two Hg^{2+} atoms is possible. It is the first example of the d^{10}−d^{10} metallophilic attraction[35,36] found in NAs.[14]

Some features of the infrared (IR) and Raman spectra measured for a 2:1 crystalline complex of 1-methylthymine with Hg^{2+} were interpreted using a simplified model of the thymine moiety.[37] Formation of the T−Hg−T base pairs in a DNA duplex upon the addition of $Hg(ClO_4)_2$ caused specific changes in the Raman spectra.[13] Similar spectral changes were observed also for the 1:1 complex of thymidylyl (3′−5′) thymidine (TpT) with Hg^{2+}, $(TpT{\cdot}Hg)_2$.[13] Characteristic bands in the C═O stretching region (near 1600 cm^{-1}) were explained by a redistribution of the charge in the thymine base upon Hg^{2+} coordination, involving partial enolization of the carbonyl group and partial covalent character of the Hg−N bond.

However, other spectral changes upon the complexation observed within the entire spectral region (~200−1800 cm^{-1}) were not explained. Signals of the sugar and phosphate parts were neglected in the T−Hg−T simplified model. Neither was it clear whether the ideally matching double helical-like structure of the $(TpT{\cdot}Hg)_2$ complex is stable and compatible with the Raman spectra measured. To answer these questions, we employed the T−Hg−T model as well as the full $(TpT{\cdot}Hg)_2$ system in the theoretical analysis. Computed harmonic force field was decomposed into the vibrational local coordinates that sensitively reflect the changes in electronic distribution upon complexation. We find that the theoretical modeling helps to rationalize the spectral interpretations and provides additional information about the heavy metal−DNA complex structure and stability.

METHODS

Raman Spectroscopy. The details about the measurement are given elswhere.[13,15] Briefly, a backscattered Raman spectra of TpT were recorded using a TpT 10 mM solution in the presence or absence of 1.75 mol equiv of $Hg(ClO_4)_2$. Each sample was sealed in a glass capillary and excited with the 514.5 nm line of a Coherent Innova 70 Ar^+ laser, using a Jasco NR-1800 spectrometer, at 295 K.

Calculations. Geometries of 1-methylthymine (T), T−Hg−T base pair, TpT dinucleotide, and the $(TpT{\cdot}Hg)_2$ complex (Figure 1) were optimized at the B3LYP/6-31+G(d,p) level of theory.[38,39] The Grimme dispersion correction[40] (DFT-D2), ultrafine grid for numerical DFT integration, and the conductor-like screening solvation model[41−43] (COSMO) were used as implemented in the Gaussian program.[44] The DFT-D2 parameters were completed by the newer DFT-D3[45] values for mercury, C_6 = 20.87 J·nm^6·mol^{-1} and R_0 = 1.68 Å. The B3LYP functional provided excellent agreement between computed and experimental spectra in the entire range of frequencies even for rather sizable systems in the past.[46−48] Standard B-DNA parameters were used to construct initial TpT and $(TpT{\cdot}Hg)_2$ geometries for the optimizations. The core electrons of the mercury atom were approximated with the relativistic pseudopotential MWB60,[49] while the valence electrons were

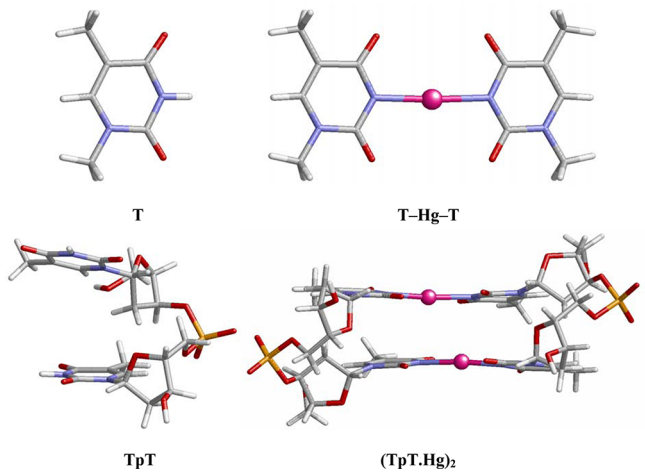

Figure 1. Computational models including 1-methylthymine (T), the T−Hg−T complex, TpT dinucleotide, and the $(TpT{\cdot}Hg)_2$ complex.

treated using the associated MWB60 basis set. Other effective core potentials, LANL2DZ[50] and MDF,[49] were also tested and provided similar results as MWB60.

The $(TpT{\cdot}Hg)_2$ geometry was alternatively optimized using the B3LYP (dispersion-uncorrected) and resolution of identity (RI) MP2[51−53] methods with the Turbomole[42] program. In RI-MP2, the 1s electrons on heavy atoms (and those replaced by the pseudopotential on Hg) were not correlated. In both cases, the def2-TZVPP basis[54] and MWB60 pseudopotential for mercury, the def-SV(P) basis set[55] for the other atoms, and the COSMO water environment were used. The C_2 symmetry was maintained during the optimization. Harmonic frequencies were calculated (numerically for MP2, analytically for DFT) at the same level as the optimizations to verify the equilibrium structures.

Harmonic vibrational frequencies and backscattered Raman intensities[56] were calculated at the same level of theory as was used for geometry optimizations. The calculated line spectra were multiplied by the temperature factor[57] and convoluted with Lorentzian band shapes of 10 cm^{-1} full-width at half-height. Natural atomic orbital Wiberg bond indexes were calculated at the B3LYP/6-31+G(d,p)/COSMO(water) level with the NBO 5.9 program linked to Gaussian.

Force Field Analysis. To be able to analyze the force field in terms of the usual chemical intrinsic coordinates (denoted by I_i, i = 1, ..., M)[58] we introduce a generalized internal force field. Deviations of the intrinsic coordinates from their equilibrium values were collected in a matrix denoted as $\mathbf{\Delta I}$. Similarly, the Cartesian coordinates X_a, a = 1, ..., N, N = 3 × number of atoms, were associated with the deviation matrix $\mathbf{\Delta X}$, which is related to the internal coordinates by a linear transformation[58,59]

$$\mathbf{\Delta I} = \mathbf{B}\mathbf{\Delta X} \tag{1}$$

Molecular force field is defined as a matrix of second energy derivatives with respect to the coordinates. Only for special cases the internal coordinate force field can be obtained directly from the Cartesian one; in general, however, the $\mathbf{B}$ matrix cannot be inverted.[58] Therefore, we look for an internal coordinate force field $\mathbf{F}_I$ that provides the best approximation to the exact Cartesian force field $\mathbf{F}_C$ minimizing

$$\sigma = (\mathbf{B}^t\mathbf{F}_I\mathbf{B} - \mathbf{F}_C)^2 + \alpha\mathbf{F}_I^2 \rightarrow \min \tag{2}$$

dx.doi.org/10.1021/jp3045077 | J. Phys. Chem. A 2012, 116, 8313−8320

where the parameter α was added for numerical stability. Tests with double-precision (8 byte) real numbers showed that the results do not depend on α within a wide range of about 10^{-10}–10^{-4}; $\alpha = 10^{-7}$ was used as a default. By setting the derivative of σ with respect to a $F_{I,op}$ component to zero, we obtain

$$\sum_{i=1}^{N}\sum_{l=1}^{N}\sum_{j=1}^{M}\sum_{k=1}^{M} B^{t}_{io}B_{pl}B^{t}_{ij}F_{I,jk}B_{kl} + \alpha F_{I,op} = \sum_{i}^{N}\sum_{l}^{N} B^{t}_{io}B_{pl}F_{C,il} \quad (3)$$

which can be rewritten as a matrix equation $\mathbf{AF}_I = \mathbf{C}$, where $A_{jk,po} = \sum_{i,l} B^{t}_{io}B_{pl}B^{t}_{ij}B_{kl} + \alpha\delta_{jk,po}$, and $C_{po} = \sum_{i,l} B^{t}_{io}B_{pl}F_{C,il}$, so that the desired internal force field is

$$\mathbf{F}_I = \mathbf{A}^{-1}\mathbf{C} \quad (4)$$

This definition allows for a redundant definition ($M > N - 6$) of the intrinsic coordinates. From $\mathbf{F}_I$, the normal mode vibrational frequencies can be obtained, for example, by the Wilson's GL method.[60,61] For the analysis of internal force field, we used diagonal elements of the intrinsic force field only, which were obtained by the same procedure (eq 4) but with significantly smaller (e.g., $M \times M$ instead of $M^2 \times M^2$ for $\mathbf{A}$) matrixes, $A_{k,o} = \sum_{i,l} B^{t}_{io}B_{ol}B^{t}_{ik}B_{kl} + \alpha\delta_{k,o}$, and $C_o = \sum_{i,l} B^{t}_{io}B_{ol}F_{C,il}$. All other vibrational properties (spectra) were calculated with the full Cartesian force field.

RESULTS AND DISCUSSION

$(TpT{\cdot}Hg)_2$ Geometry. As pointed out many times previously,[62,63] the HF and early DFT methods do not describe the dispersion attraction well. Fortunately, significant improvement can be easily achieved by empirical corrections.[40,45,64,65] Indeed, as follows from the comparison of the complex geometries obtained with different approximation levels (Figure 2), the correction provides realistic geometry of the dinucleotide–mercury complex.

The B3LYP calculation without the dispersion correction provides unrealistic $(TpT{\cdot}Hg)_2$ geometry, with a very long Hg···Hg distance ($d_{Hg\cdots Hg}$ = 7.67 Å). Inclusion of the DFT-D2 correction results to the Hg···Hg distance of 3.52 Å, which is reasonably close to the 3.28 Å obtained at the supposedly more reliable RI-MP2 level. As the MP2 wave function method is known to slightly overestimate the dispersion interaction,[63] the MP2 value of 3.28 Å can be considered a lower limit for the Hg···Hg distance, while the DFT-D2 value of 3.52 Å may be more realistic. Note also that the base pairs in the MP2 structure are not as coplanar as for DFT-D2; the predicted twist between the base planes in a base pair is about 36° and 12° for MP2 and DFT-D2, respectively.

The results can be hampered by the incomplete basis set that had to be used for these large systems ; however, from previous studies, we know that the effect on the geometry is rather minor (unlike for conformational energies) and that the basis set with diffuse and polarization functions used in this study is sufficient to model conformational behavior of the DNA segments.[14]

Interestingly, the DFT-D2 and MP2 $d_{Hg\cdots Hg}$ values are within the usual base-pair separation (3.2–3.6 Å) observed[66–70] or predicted[71,72] for much lighter metals incorporated to DNA, such as potassium or sodium intercalated between DNA bases. More importantly, the metal-mediated base pair separation obtained with DFT-D2 is quite close to natural interbase separations observed in B-DNA.[73] In other words, the metallophilic[14] and the metal–base pair attractions to a large degree minimize the perturbation introduced to the natural DNA structure by the mercury.

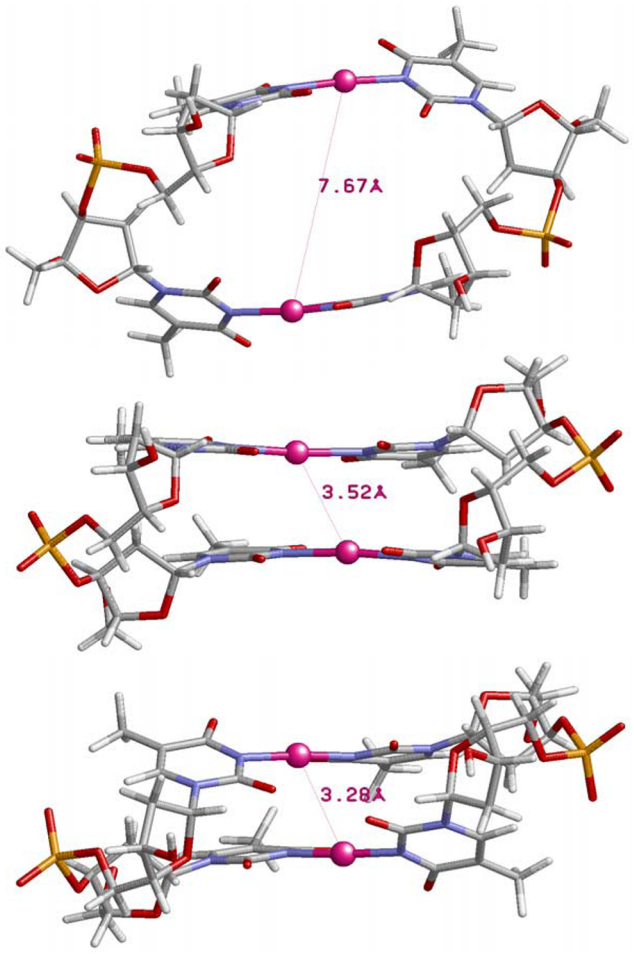

Figure 2. $(TpT{\cdot}Hg)_2$ complex optimized at the B3LYP/COSMO (top), B3LYP-D2/COSMO (middle), and RI-MP2/COSMO (bottom) approximation levels.

The Hg–N distances and N–Hg–N angles obtained with three pseudopotentials are listed in Table 1 (columns 2–4). While the variations up to ~10% in the Hg–N distance occur, the N–Hg–N linkage remains nearly linear. These results are in agreement with the X-ray geometry of T–Hg–T[15] (last column of the table). The addition of the COSMO solvent causes a lengthening of the Hg–N bond, e.g., from 2.069 to 2.153 Å for the MWB60 pseudopotential, i.e., the bond becomes weaker. The vacuum values are closer to the experimental bond lengths than for COSMO; most probably, this is caused both by inadequacy of the water COSMO environment for the crystal and the tendency of DFT to overestimate the bond length. Indeed, trial MP2 computations (not shown) provided shorter Hg–N bond length, in favor of experiment. The basis set variation on the bases (columns 5–6 in Table 1) has a little effect on the geometry near Hg, e.g., the bond length of 2.135 Å for 6-31G** becomes longer to 2.157 Å for 6-311++G**, etc. The Hg–N bond also becomes slightly longer when the dispersion is added (cf. columns 4 and 7).

Vibrations of the T–Hg–T Moiety. First, we used the simplified T–Hg–T system to investigate the most important vibrational motions related to the Hg–DNA binding. Relevant modes can be approximately divided to those associated

dx.doi.org/10.1021/jp3045077 | J. Phys. Chem. A 2012, 116, 8313–8320

Table 1. Geometry Parameters of the N−Hg−N Link in T−Hg−T Calculated with Various Methods

DFT method	B3LYP	B3LYP	B3LYP	B3LYP	B3LYP	B3LYP-D2	
atomic basis	6-31+G**	6-31+G**	6-31+G**	6-31G**	6-311++G**	6-31+G**	
Hg pseudopotential and basis	LANL2DZ	MDF	MWB60	MWB60	MWB60	MWB60	exptl[b]
d(Hg−N) (Å)[a]	2.238/2.309	2.095/2.224	2.069/2.153	2.064/2.135	2.071/2.157	2.091/2.183	2.035
∠N−Hg−N (deg)[a]	160/179	177/177	179/176	179/177	179/176	179/177	180

[a]Without/with the COSMO solvent. [b]CSD ID code MTYMHG10, T−Hg−T, ref 15.

directly with the Hg−N3 bonds, and to those predominantly located on thymine. Most distinct vibrational mode displacements are plotted in Figure 3. For example, the almost pure in-phase Hg−N stretching (mode number 9) is quite decoupled from the thymine motion, and only a weak coupling can be seen between the Hg−N out of phase stretching and a methyl wagging (mode number 17). However, there is a strong coupling between the Hg−N and C−N thymine stretches in the mode 36.

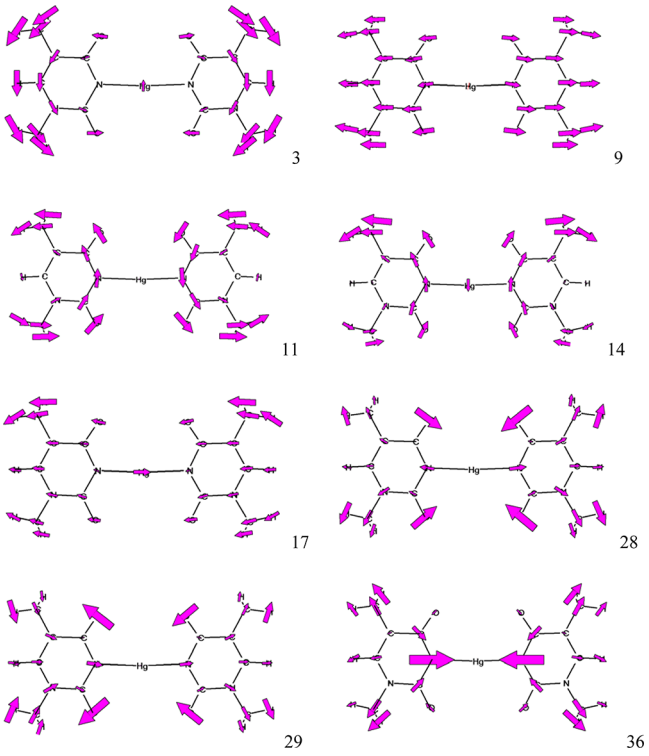

Figure 3. Example of calculated vibrational modes in T−Hg−T most affected by the N3−Hg−N3 link.

The theoretical vibrational frequencies and Raman intensities of the mercury link modes are fairly independent of the pseudopotential used (Table 2); for MWB60, LANL2DZ, and MDF, the differences of the modes associated with the Hg−N bond (e.g., modes 9 and 17) are quite minor, ∼±10 cm^{-1}. The lowest-frequency mode is influenced more, and its frequency is even close to zero for MDF. Note that the low-frequency vibrations are in general computed less accurately.[74,75] However, this has little implications as such modes are not easily measurable. More significant differences appear for the relative Raman intensities (I) and the depolarization ratios (η) (Table 2) of higher-frequency modes (>10 cm^{-1}). For other approximations (BPW91, other basis sets, not shown) the vibrational Raman behavior was quite similar.

Frequency and Raman Intensity Changes upon Mercury Binding. For selected thymine vibrational modes, the predicted changes of frequencies and isotropic backscattering Raman intensities upon mercury binding are summarized in Table 3. We can see that the mercury causes vibrational mode frequency shifts within a wide range, from −80 to +54 cm^{-1}. The intensities listed in Table 3 are affected especially for modes at 389, 525, 783, and 1246 cm^{-1}. In accordance with the previous observation,[13] the most extreme shift occurs for the C=O stretching mode at 1685 cm^{-1}. This mode also significantly loses its Raman intensity upon the Hg^{2+} binding.

The entire calculated Raman spectral profiles for the T−Hg−T and $(TpT{\cdot}Hg)_2$ models are compared to experiment in Figure 4. For T−Hg−T (upper part of Figure 4), the calculation is compared to the experimental Raman spectra redrawn from ref 37, the $(TpT{\cdot}Hg)_2$ complexation is followed at the lower part of the figure. Although the mercury attachment causes rather complex changes in the Raman spectral pattern, most of the shifts were reproduced by the calculations. The changes below 400 cm^{-1} may be affected by the baseline subtraction and other experimental artifacts.[76] In

Table 2. Vibrational Modes Associated with the N−Hg−N Link in T−Hg−T, Frequencies (ν/cm^{-1}), Raman Backscattering Intensities (I/au), and Depolarization Ratios (η) Calculated with the B3LYP/6-31+G/COSMO Method Employing Three Pseudopotentials for Mercury**

		LANL2DZ			MDF			MWB60		
mode		ν (cm^{-1})	I	η	ν (cm^{-1})	I	η	ν (cm^{-1})	I	η
3	A′	22	4	0.10	0	1	0.74	49	1	0.53
9	A′	125	38	0.32	114	50	0.28	126	103	0.25
11	A′	27	1	0.75	99	14	0.72	136	15	0.75
14	A′	46	6	0.10	125	2	0.11	173	1	0.50
17	A′	174	1	0.75	182	0	0.46	195	1	0.73
28	A′	429	28	0.47	427	24	0.42	440	99	0.45
29	A′	430	6	0.47	420	59	0.44	441	1	0.42
36	A′	742	160	0.39	737	88	0.49	747	304	0.32

dx.doi.org/10.1021/jp3045077 | J. Phys. Chem. A 2012, 116, 8313−8320

Table 3. Frequencies (cm^{-1}) and Raman Intensities ($Å^4$/amu) of Thymine Vibrational Modes (Without Modes Localized on Methyl Groups and NH out of Plane Motion), and Their Changes upon the Hg^{2+} Binding in the T−Hg−T Complex, Calculated at the B3LYP-D2/6-31+G/COSMO(water) Level; the MWB60 Pseudopotential and Basis Set Were Used for Mercury**

ω_T	$\omega_{THgT} - \omega_T$	I_T	$I_{THgT}/2 - I_T$	vibrational mode
212	25	3	0	ring out of plane (oop)
271	11	2	0	ring oop
309	−1	4	1	ring oop
389	51	9	25	C═O sym. bend
412	23	10	0	ring oop
451	12	30	−1	ring def.
525	12	120	84	ring def.
656	24	21	−5	C═O asym. bend
698	53	52	44	ring def.
751	6	0	0	C═O oop
762	7	14	−5	C═O oop
783	3	157	19	ring def.
883	54	32	9	ring def.
922	−4	26	2	C−H oop
1157	28	20	−7	ring def.
1209	1	71	100	ring def.
1246	12	158	240	ring def.
1355	8	66	−49	ring def.
1391	−7	533	−49	ring def.
1415	−1	172	−20	ring def., CH, NH bends
1685	−82	257	−134	ν(C═O)
1689	7	912	−397	ν(C═C)
1726	−55	319	−28	ν(C═O)

particular, we assign the band at 319 cm^{-1} to the Hg−triethylamine (TEA) complex for $(TpT{\cdot}Hg)_2$. Some regions can be attributed to the signal of the ClO_4^- ion.

The changes of Raman frequencies and intensities caused by the mercury binding are mostly subtle. Most changes observed for the simpler T/T−Hg−T system can be related to those for $TpT/(TpT{\cdot}Hg)_2$. For example, the most characteristic band analyzed already in our previous work[13] appears around 1587 cm^{-1} both for T−Hg−T and $(TpT{\cdot}Hg)_2$. However, the signal of $(TpT{\cdot}Hg)_2$ is clearly more complex, and we see that the sugar−phosphate residue and the stacking interactions included in the complete model of the complex are important for obtaining correct spectral intensities for the mercury-mediated dinucleotide.

In detail, the calculated and experimental vibrational frequency shifts of the most intense Raman bands are summarized in Table 4. As in Figure 4, the simplified T−Hg−T system reproduces the changes in $(TpT{\cdot}Hg)_2$ only approximately. The computations provide most of the observed frequency changes correctly, within a few cm^{-1}, including the 1587 cm^{-1} (1664 − 77 cm^{-1}, C═O stretching, Table 4) band at $(TpT{\cdot}Hg)_2$. Mostly, the thymine modes are influenced by the binding (cf. Tables 3 and 4); we do not attempt to assign the sugar−phosphate modes as they are less specific, supposedly not much influenced by the mercury binding, but contribute to a background Raman scattering within the entire region of wavenumbers (Figure 4). A tentative assignment of the TpT Raman bands based on the comparison of the spectral intensities (Figure 4) and dynamic visualization of the calculated normal mode displacement are summarized in Table 5. For the bands at 748, 1664, and 1687 cm^{-1}, the assignment is consistent with the characterization based on

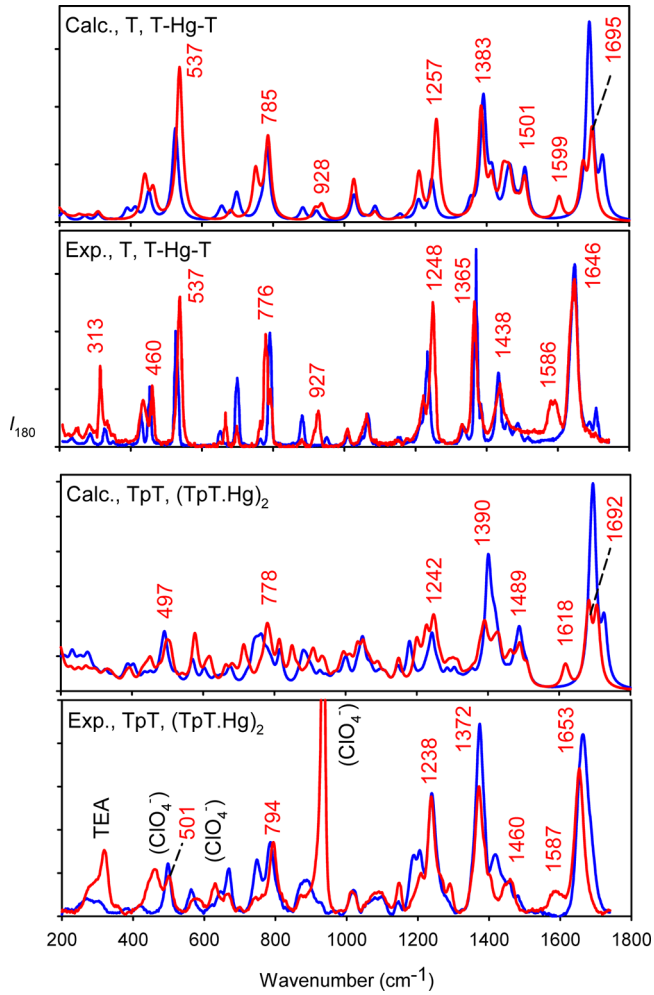

Figure 4. Raman spectra, from top to bottom: calculated for T (blue, intensity multiplied by two) and T−Hg−T (red), experimental spectra of T (blue) and T−Hg−T (red) from ref 37, calculation for TpT (blue, ×2) and $(TpT{\cdot}Hg)_2$ (red), and experimental Raman spectra of pure 10 mM TpT (blue) and after the addition of 17.5 mM $Hg(ClO_4)_2$ (red). Main bands of the mercury complexes, the ClO_4^- ion, and Hg−triethylamine complex (TEA) are labeled.

Table 4. Calculated (B3LYP-D2/6-31+G/COSMO) and Experimental Frequencies of Selected Raman Bands in TpT (cm^{-1}) and Frequency Changes upon Hg^{2+} Binding**

ω_{TpT}		$\omega_{THgT} - \omega_T$		$\omega_{(TpT{\cdot}Hg)_2} - \omega_{TpT}$	
calcd	exptl	calcd	exptl[a]	calcd	exptl
491	498	12	10	9	3
570	563	12	13	7	15
763	786	2	−12	18	8
1146	1146			3	2
1243	1239	12	14	4	−1
1401	1374	−7	−4	−11	−2
1421	1418	−1	5	6	−18
1488	1481			1	−22
1695	1664	−82	−60	−77	−77
1726	1687	−55	−60	−42	−34

[a]Reference 37.

dx.doi.org/10.1021/jp3045077 | J. Phys. Chem. A 2012, 116, 8313−8320

Table 5. Frequencies of the Strongest TpT Raman Peaks and Tentative Assignment

ω_{TpT}, exptl	
270, 303, 420	ring oop
385	C═O sym. bend
498, 563, 670	ring def.
644	C═O asym. bend
748	C═O oop
786, 881, 1019	ν(C−C), delocalized modes
1079, 1099	in phase ν(P═O), sugar modes
1146, 1189	ring def.
1205	out of phase ν(P═O), sugar modes
1239, 1374	ring def.
1418, 1454, 1481	ring def., CH, NH bends, CH_2 scissor
1664, 1687 (shoulder)	ν(C═O), ν(C═C)

experiment,[13] except for the 748 cm^{-1} attributed to imino proton in ref 13.

The theoretical values of the frequency shifts are usually slightly overestimated, which can be explained by neglecting the effects of dynamics and explicit solvent.[77,78] Modeling of these effects is currently not affordable for the system as large as $(TpT{\cdot}Hg)_2$. Overall, however, we can conclude that the simulations can explain most of the observed changes and thus link the Raman spectral variations to the mercury binding to TpT dinucleotide.

Changes in Molecular Force Field. As suggested previously,[13] the binding of mercury to DNA causes relatively large changes in the electronic structure and consequent variations in internal molecular force field. As can be seen in Figure 5, the replacement of the thymine imino hydrogen by

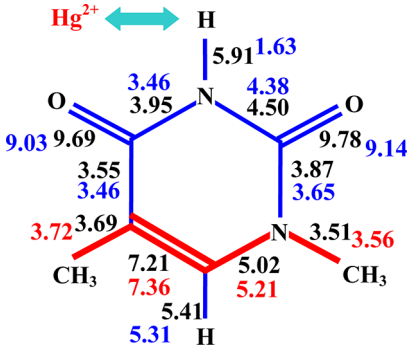

Figure 5. Calculated changes in internal coordinate force field (blue, weakening; red, strengthening, only stretching constants are listed, in au) of 1-methylthymine after Hg^{2+} binding.

mercury causes a uniform weakening of the stretching constants in its vicinity (blue bonds), and strengthening of the more remote bonds (red). Up to 10% change occurs for the C═O bond force constant, which is also in agreement with the partial enol character of C═O and a partial covalent character of the Hg−N3 bonds suggested previously.[13] Obviously, the Hg−N bond (with the intrinsic force constant f = 1.63 au) is still much weaker than the N−H bond (f = 5.91 au).

The mercury ion clearly causes a significant charge redistribution in the thymine ring, which can be also documented by the correlation of the force constants changes with the formal bond order differences plotted in Figure 6. The largest changes in the NBO bond order (~0.1) correspond to the largest change of the internal force constants (~1.5 au).

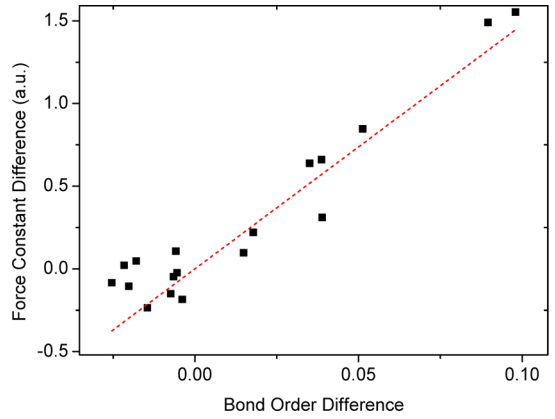

Figure 6. Correlation between changes of stretching force constants and natural bond order changes upon Hg^{2+} binding to 1-methylthymine.

The vibrational spectroscopy thus reveals information about the changes in the electronic structure upon the binding, reflected in the Raman spectral intensities, frequencies, and underlying mechanical properties of the molecule.

CONCLUSIONS

We have used several quantum chemical models to calculate the frequency and intensity changes in the Raman spectra that were previously observed in the TpT dinucleotide upon the Hg^{2+} binding. We have shown that the B-DNA-like dimer $(TpT{\cdot}Hg)_2$ geometry is theoretically possible within the DFT and MP2 methodologies and that the van der Waals Hg···Hg and Hg···base attractions stabilize this structure. Thus, also this interaction, in the addition to the π-electronic attraction of the base pairs, has to be considered in theoretical modeling of DNA structures.

The mercury binding to DNA caused many intensity and frequency changes in the Raman spectra. Some of the variations, such as slight frequency shifts, were not immediately apparent from the spectral shape, and some of them were obscured by the perchlorate signal. However, when compared to the calculations, most of the changes could be related to the $(TpT{\cdot}Hg)_2$ vibrational normal modes, and the most important frequency shifts could be qualitatively reproduced. The simplified T−Hg−T model provided qualitatively correct spectra, whereas including the influence of the base stacking and the sugar−phosphate residue in $(TpT{\cdot}Hg)_2$ improved the reliability of the prediction. The Raman spectroscopy is a convenient and reproducible tool for the monitoring of DNA−mercury interactions.

AUTHOR INFORMATION

Corresponding Author

*E-mail: bour@uochb.cas.cz.

Notes

The authors declare no competing financial interest.

ACKNOWLEDGMENTS

The study was performed with the support from the Grant Agency (P208/11/0105, P206/12/0539, and 205/10/0228) and Ministry of Education (LH11033) of the Czech Republic.

REFERENCES

(1) Tanaka, K.; Tengeiji, A.; Kato, T.; Toyama, N.; Shionoya, M. *Science* **2003**, *299*, 1212−1213.
(2) Wagenknecht, H. A. *Angew. Chem., Int. Ed.* **2003**, *42*, 3204−3206.
(3) Shionoya, M.; Tanaka, K. *Curr. Opin. Chem. Biol.* **2004**, *8*, 592−597.
(4) Miyake, Y.; Togashi, H.; Tashiro, M.; Yamaguchi, H.; Oda, S.; Kudo, M.; Tanaka, Y.; Kondo, Y.; Sawa, R.; Fujimoto, T.; et al. *J. Am. Chem. Soc.* **2006**, *128*, 2172−2173.
(5) Tanaka, K.; Shionoya, M. *Coord. Chem. Rev.* **2007**, *251*, 2732−2742.
(6) Clever, G. H.; Kaul, C.; Carell, T. *Angew. Chem., Int. Ed.* **2007**, *46*, 6226−6236.
(7) Müller, J. *Eur. J. Inorg. Chem.* **2008**, 3749−3763.
(8) Liu, J.; Cao, Z.; Lu, Y. *Chem. Rev.* **2009**, *109*, 1948−1998.
(9) Johannsen, S.; Megger, N.; Bohme, D.; Sigel, R. K. O.; Muller, J. *Nat. Chem.* **2010**, *2*, 229−234.
(10) Clever, G. H.; Shionoya, M. *Coord. Chem. Rev.* **2010**, *254*, 2391−2402.
(11) Chiba, J.; Inouye, M. *Chem. Biodiversity* **2010**, *7*, 259−282.
(12) Ono, A.; Torigoe, H.; Tanaka, Y.; Okamoto, I. *Chem. Soc. Rev.* **2011**, *40*, 5855−5866.
(13) Uchiyama, T.; Miura, T.; Takeuchi, H.; Dairaku, T.; Komuro, T.; Kawamura, T.; Kondo, Y.; Benda, L.; Sychrovský, V.; Bouř, P.; et al. *Nucleic Acids Res.* **2012**, *40*, 5766−5774.
(14) Benda, L.; Straka, M.; Tanaka, Y.; Sychrovský, V. *Phys. Chem. Chem. Phys.* **2011**, *13*, 100−103.
(15) Tanaka, Y.; Oda, S.; Yamaguchi, H.; Kondo, Y.; Kojima, C.; Ono, A. *J. Am. Chem. Soc.* **2007**, *129*, 244−245.
(16) Tanaka, Y.; Ono, A. *Dalton Trans.* **2008**, *37*, 4965−4974.
(17) Katz, S. *J. Am. Chem. Soc.* **1952**, *74*, 2238−2245.
(18) Yamane, T.; Davidson, N. *J. Am. Chem. Soc.* **1961**, *83*, 2599−2607.
(19) Gruenwedel, D. W.; Cruikshank, M. K. *Nucleic Acids Res.* **1989**, *17*, 9075−9086.
(20) Gruenwedel, D. W.; Cruikshank, M. K. *Biochemistry* **1990**, *29*, 2110−2116.
(21) Gruenwedel, D. W.; Cruikshank, M. K. *Inorg. Chem.* **1991**, *43*, 29−36.
(22) Gruenwedel, D. W.; Cruikshank, M. K.; Smith, G. M. *Inorg. Chem.* **1993**, *52*, 251−261.
(23) Izatt, R. M.; Christen, J. J.; Rytting, J. H. *Chem. Rev.* **1971**, *71*, 439−481.
(24) Simpson, R. B. *J. Am. Chem. Soc.* **1964**, *86*, 2059−2065.
(25) Katz, S. *Biochim. Biophys. Acta* **1963**, *68*, 240−253.
(26) Young, P. R.; Nandi, U. S.; Kallenbach, N. R. *Biochemistry* **1982**, *21*, 62−66.
(27) Kuklenyik, Z.; Marzilli, L. G. *Inorg. Chem.* **1996**, *35*, 5654−5662.
(28) Tanaka, Y.; Yamaguchi, H.; Oda, S.; Kondo, Y.; Nomura, M.; Kojima, C.; Ono, A. *Nucleosides, Nucleotides Nucleic Acids* **2006**, *25*, 613−624.
(29) Ono, A.; Togashi, H. *Angew. Chem., Int. Ed.* **2004**, *43*, 4300−4302.
(30) Lee, J. S.; Ulmann, P. A.; Han, M. S.; Mirkin, C. A. *Nano Lett.* **2008**, *8*, 529−533.
(31) Johannsen, S.; Paulus, S.; Dupre, N.; Muller, J.; Sigel, R. K. O. *Inorg. Biochem.* **2008**, *102*, 1141−1151.
(32) Voityuk, A. A. *J. Phys. Chem. B* **2006**, *110*, 21010−21013.
(33) Joseph, J.; Schuster, G. B. *Org. Lett.* **2007**, *9*, 1843−1846.
(34) Miyachi, H.; Matsui, T.; Shigeta, Y.; Hirao, K. *Phys. Chem. Chem. Phys.* **2010**, *12*, 909−917.
(35) Pyykkö, P. *Chem. Rev.* **1997**, *97*, 597−636.
(36) Pyykkö, P.; Straka, M. *Phys. Chem. Chem. Phys.* **2000**, *2*, 2489−2493.
(37) Morzyk-Ociepa, B.; Michalska, D. *J. Mol. Struct.* **2001**, *598*, 133−144.
(38) Becke, A. D. *J. Chem. Phys.* **1993**, *98*, 5648−5652.
(39) Lee, C.; Yang, W.; Parr, R. G. *Phys. Rev. B* **1988**, *37*, 785−789.
(40) Grimme, S. *J. Comput. Chem.* **2006**, *27*, 1787−1799.
(41) Klamt, A.; Schuurmann, G. *J. Chem. Soc., Perkin Trans.* **1993**, *2*, 799−805.
(42) Barone, V.; Cossi, M. *J. Phys. Chem. A* **1998**, *102*, 1995−2001.
(43) Cossi, M.; Rega, N.; Scalmani, G.; Barone, V. *J. Comput. Chem.* **2003**, *24*, 669−681.
(44) Frisch, M. J.; Trucks, G. W.; Schlegel, H. B.; Scuseria, G. E.; Robb, M. A.; Cheeseman, J. R.; Scalmani, G.; Barone, V.; Mennucci, B.; Petersson, G. A.; et al. *Gaussian 09*, revision B.01; Gaussian, Inc.: Wallingford CT, 2009.
(45) Grimme, S.; Antony, J.; Ehrlich, S.; Krieg, H. *J. Chem. Phys.* **2010**, *132*, 154104.
(46) Zvereva, E. E.; Shagidullin, A. R.; Katsyuba, S. A. *J. Phys. Chem. A* **2011**, *115*, 63−69.
(47) Yamamoto, S.; Kaminský, J.; Bouř, P. *Anal. Chem.* **2012**, *84*, 2440−2451.
(48) Yamamoto, S.; Straka, M.; Watarai, H.; Bouř, P. *Phys. Chem. Chem. Phys.* **2010**, *12*, 11021−11032.
(49) Figgen, D.; Rauhut, G.; Dolg, M.; Stoll, H. *Chem. Phys.* **2005**, *311*, 227−244.
(50) Hay, P. J.; Wadt, W. R. *J. Chem. Phys.* **1985**, *82*, 299−310.
(51) Weigend, F.; Haser, M. *Theor. Chem. Acc.* **1997**, *97*, 331−340.
(52) Weigend, F.; Haser, M.; Patzelt, H.; Ahlrichs, R. *Chem. Phys. Lett.* **1998**, *294*, 143−152.
(53) del Valle, F. J. O.; Tomasi, J. *Chem. Phys.* **1991**, *150*, 139−150.
(54) Weigend, F.; Ahlrichs, R. *Phys. Chem. Chem. Phys.* **2005**, *7*, 3297−3305.
(55) Schäfer, A.; Horn, H.; Ahlrichs, R. *J. Chem. Phys.* **1992**, *97*, 2571−2577.
(56) Nafie, L. *Vibrational Optical Activity: Principles and Applications*; Wiley: Chichester, U.K., 2011.
(57) Polavarapu, P. L. *Vibrational Spectra: Principles and Applications with Emphasis on Optical Activity*; Elsevier: Amsterdam, The Netherlands, 1998; Vol. *85*.
(58) Wilson, E. B.; Decius, J. C.; Cross, P. C. *Molecular Vibrations*; Dover: New York, 1980.
(59) Papoušek, D.; Aliev, M. R. *Molecular Vibrational/Rotational Spectra*; Academia: Prague, Czech Republic, 1982.
(60) Wilson, E. B. *J. Chem. Phys.* **1939**, *7*, 1047−1052.
(61) Shimanouchi, T.; Tsuboi, M. *J. Chem. Phys.* **1961**, *35*, 1597−1612.
(62) Hobza, P.; Šponer, J. *Chem. Rev.* **1999**, *99*, 3247−3276.
(63) Šponer, J.; Hobza, P. *Collect. Czech. Chem. Commun.* **2003**, *68*, 2231−2282.
(64) Grimme, S. *J. Comput. Chem.* **2004**, *25*, 1463−1473.
(65) Parchaňský, V.; Matějka, P.; Dolenský, B.; Havlík, M.; Bouř, P. *J. Mol. Struct.* **2009**, *934*, 117−122.
(66) Arnott, S.; Chandrasekaran, R.; Marttila, C. M. *Biochem. J.* **1974**, *141*, 537−543.
(67) Wang, Y.; Patel, D. J. *J. Mol. Biol.* **1993**, *234*, 1171−1183.
(68) Keniry, M. A.; Strahan, G. D.; Owen, A.; Shafer, R. H. *Eur. J. Biochem.* **1995**, *233*, 631−643.
(69) Schultze, P.; Smith, F. W.; Feigon, J. *Structure* **1994**, *2*, 221−233.
(70) Haider, S.; Parkinson, G. N.; Neidle, S. *J. Mol. Biol.* **2002**, *320*, 189−200.
(71) Andrushchenko, V.; Tsankov, D.; Krasteva, M.; Wieser, H.; Bouř, P. *J. Am. Chem. Soc.* **2011**, *133*, 15055−15064.
(72) Chowdhury, S.; Bansal, M. *J. Phys. Chem. B* **2001**, *105*, 7572−7578.
(73) Saenger, W. *Principles of Nucleic Acid Structure*; Springer-Verlag: Berlin, Germany, 1984.
(74) Scott, A. P.; Radom, L. *J. Phys. Chem.* **1996**, *100*, 16502−16513.
(75) Montgomery, J. A.; Frisch, M. J.; Ochterski, J. W.; Petersson, G. S. *J. Chem. Phys.* **1999**, *110*, 2822−2827.
(76) Kapitán, J.; Dračínský, M.; Kaminský, J.; Benda, L.; Bouř, P. *J. Phys. Chem. B* **2010**, *114*, 3574−3582.
(77) Kapitán, J.; Baumruk, V.; Kopecký, V., Jr.; Bouř, P. *J. Phys. Chem. A* **2006**, *110*, 4689−4696.

(78) Hopmann, K. H.; Ruud, K.; Pecul, M.; Kudelski, A.; Dračínský, M.; Bouř, P. *J. Phys. Chem. B* **2011**, *115*, 4128−4137.